4.1. Introduction

The amide bonds are the building blocks and crucial functional groups that determine the effectiveness of many natural and synthetic polymers like peptides, proteins, and life-saving drugs.[1],[2],[3] In 2020, amide derivative drugs, particularly those with aromatic properties, constituted 73 out of the top 200 best-selling pharmaceuticals in the USA.[1],[4],[5] The amides and their different derivatives are useful intermediates in synthetic chemistry and in the industrial production of goods, including drugs, lubricants, proteins, natural products, polymers, and functional materials.[6],[7],[8],[9],[10]

In the last few decades, catalytic approaches have been explored for the selective formation of amide (O=C−N−) bond with high conversion efficiency.[11],[12] Several transition metal-based catalysts were reported for the coupling of aldehyde with amine to synthesize amides having structural diversity.[13],[14],[15] The catalytic oxidative amidation of aldehydes with amines has emerged as an attractive approach because of high atom economy, product selectivity, and readily available substrates compared to other methods.[16],[17]

The catalytic amidation reaction in the homogeneous medium includes noble metal complexes of Pd,[18],[19] Ir,[20],[21] Ru,[22],[23] Rh[24],[25],[26] etc.[27],[28] Further, transition metal-based (Ni,[29] Fe,[30] Co,[11] Cu,[16] etc.)[31] homogenous complexes were used as the catalysts for the amidation reactions but with additive ligands.[32],[29] These metal complexes catalysts provide better catalytic activity and selectivity for the amide reactions.[33] Although these catalysts produced high activity and selectivity for the oxidative amidation reaction, the typical drawback of homogenous catalysis limited their wide applications.[34] Further, the use of costly ligands, noble metals, and additives in homogeneous catalysis made it impractical.[35],[33]

In this context, the heterogeneous catalysts offered high activity and selectivity with the

benefit of recycling. For example, silica-supported Cu[36],[37] and Mn[38] catalysts have been demonstrated for the oxidative amidation reaction between aldehyde and amine.[8],[39] The Ni and Fe-based heterogeneous catalyst supported on the TiO_2 also provides better activity for the amidation reactions at high temperature.[4] However, the utilization of the M−N−C type catalysts with modulated electronic and atomic structure has never been explored for the oxidative amidation reaction.[40],[41],[42],[43],[44] As the primary objective of the thesis is to explore M−N−C type catalysts for different organic transformation reactions, we have explored Ni−N−C@NC catalysts for the oxidative amide formation of amines with aldehydes.

For this, we have synthesized MOF-derived Ni−N−C@NC (NC= nitrogen-doped carbon) catalysts (**Scheme 4.1**) and explored for the amidation reaction of amines. We have chosen Ni-ZIF-8 as the precursor and pyrolyzed it to form Ni−N−C@NC. In Ni−N−C@NC, the unique coordination of Ni−center provides excellent catalytic activity and selectivity for the amidation formation of amines with benzaldehydes to obtain the yield >98% of the amides. Further, the Ni−N−C@NC catalyst is stable for seven cycles for the amidation reactions.

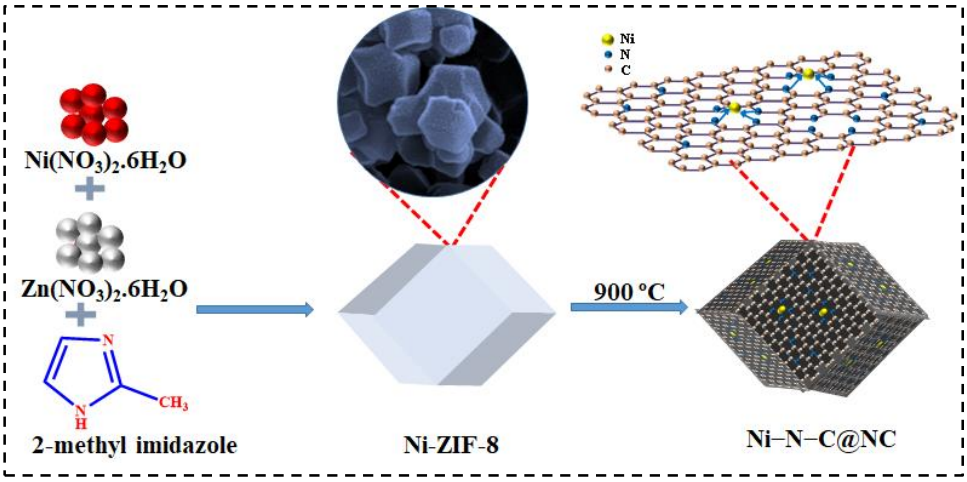

Scheme 4.1. Schematic representation of the synthesis of Ni−N−C@NC catalyst.

4.2. Chemicals

Nickel(II) nitrate hexahydrate ($Ni(NO_3)_2.6H_2O$), methanol, 1,4-dioxane and silica gel were purchased from MERCK Life Sciences Ltd. India). 2-methylimidazole was purchased from Avra Laboratories Pvt. Ltd. India. Chloroform-D was purchased from Sigma-Aldrich Pvt. Ltd., India. Benzaldehyde and primary and secondary amines were obtained from Sigma-Aldrich, Avra, Alfa Aesar and SRL Pvt. Ltd., India. All catalytic experiments were carried out in a round bottom flask (volume 25 mL, from Borosil).

4.3. Instruments

The same instruments were used for the spectroscopic, microscopic and NMR characterization of the catalysts and products as mentioned in chapter 2 section 2.3.

4.4. Experimental

4.4.1. Synthesis of Ni-ZIF-8[45],[46]

$Ni(NO_3)_2.6H_2O$ (0.3 mmol) and $Zn(NO_3)_2.6H_2O$ (0.7 mmol) were dissolved in 20 mL methanol and stirred for 10 minutes to get the solution A. 2-methylimidazole (4 mmol) was separately dissolved in 20 mL methanol and stirred for 10 minutes to get the solution B. Then, solution B was added to A at a time and stirred for 24 h at room temperature. The precipitate of Ni-ZIF-8 was obtained. The precipitate was collected by centrifugation (13000 rpm for 15 minutes) and washed five times with methanol. The obtained precipitate was dried at 60 °C in a hot air oven overnight.

4.4.2. Synthesis of ZIF-8[45]

$Zn(NO_3)_2.6H_2O$ (1 mmol) was dissolved in 20 mL methanol and stirred for 10 minutes to get the solution A. 2-methylimidazole (4 mmol) was separately dissolved in 20 mL methanol and stirred for 10 minutes to get the solution B. Same as the above process to

obtained ZIF-8.

4.4.3. Synthesis of Ni−N−C@NC[46],[47]

200 mg of Ni-ZIF-8 was ground in a mortar pestle to get a fine powder. The powder was placed in a crucible boat and heated at 900 °C in the presence of N_2 for 3 h (in a tubular furnace with heating rate: 5 °C/min from 35 °C). The furnace was allowed to cool down to room temperature. The black powder was collected and denoted as Ni−N−C@NC.

4.4.4. Synthesis of NC[47]

200 mg of ZIF-8 was taken and the previous process was applied to produce NC.

4.4.5. Synthesis of Ni@C

$Ni(NO_3)_2.6H_2O$ (0.3 mmol) were dissolved in 20 mL methanol and stirred for 10 minutes to get solution A. $NaBH_4$ (2 mmol) was dissolved in 20 mL methanol and stirred for 1 minute to form the solution B. The solution B was added to A at a time and stirred for 24 h. The mixture yielded a black suspension of Ni@C. The precipitate was collected by centrifugation (11000 rpm for 10 minutes) and washed five times with methanol. The obtained precipitate was dried at 60 °C in a hot air oven overnight.

4.5. Results and discussion

4.5.1. Characterizations of the catalyst

First, the precursor Ni-substituted zeolitic imidazolate framework-8 (Ni-ZIF-8, a type of MOF) was synthesized by the reaction of nickel(II) nitrate, zinc (II) nitrate, and 2-methylimidazole in methanol. To maintain a low loading of Ni in Ni−N−C@NC, only 30% of Zn was substituted by Ni. The powder X-ray diffraction (PXRD) of Ni-ZIF-8 showed the characteristic crystal planes of ZIF-8 (JCPDS 00-062-1030, **Figure 4.1a**)[47]

and 0.06° peak shift towards the right due to Ni doping. The field emission-scanning electron microscope (FE-SEM) showed the rhombic dodecahedron morphology of Ni−ZIF-8 (**Figure 4.1b**).[48] The EDX elemental mapping revealed the homogeneous distribution Ni, Zn, N, and C of the elements (**Figure 4.1c-f**).[48]

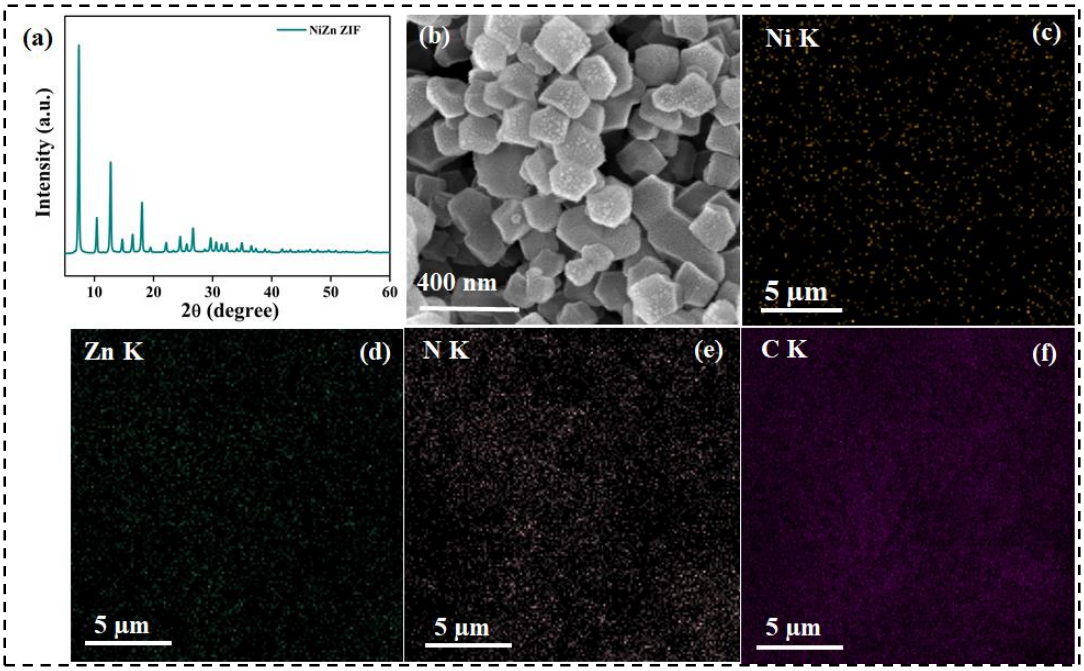

Figure 4.1: (a) PXRD pattern of Ni−ZIF-8, (b) FE-SEM image with rhombic dodecahedron morphology. (c-f) Elemental mapping of Ni−ZIF-8 (with elements: Ni, Zn, N, and C).

Next, Ni−ZIF-8 was pyrolyzed in N_2 atmosphere at 900 °C to form Ni−N−C@NC. The variation of the pyrolysis temperature (700 and 800 °C) produced NiZn−N−C@NC−700 and NiZn−N−C@NC−800, respectively. During the pyrolysis of Ni−ZIF-8, the Zn undergoes sublimation above 700 °C and the complete sublimation of Zn was achieved at 900 °C, producing Ni−N−C@NC.[49]

The PXRD pattern of Ni−N−C@NC detected two broad diffraction peaks at 2θ = 24.1° and 42.9° (**Figure 4.2a**) which were indexed for the (002) and (101) planes of

graphitized carbon.[50] The peaks corresponding to fcc or hcp Ni were not detected by PXRD because of low loading of Ni as well as ultra-small particle size (< 1nm, see later).

Further, the graphitic nature of the NC support was confirmed by Raman spectroscopy. The Raman spectra of Ni−N−C@NC revealed peaks at 1326 and 1584 cm^{-1}, corresponding to D and G bands of graphene, respectively (**Figure 4.2b**). The I_D/I_G ratio of 1.44 indicates the defect-rich graphitic carbon structure with the presence of sp^2 and sp^3 carbons. The 2D band appeared at 2555 cm^{-1} whereas peak for C−N bond was detected at 2074 cm^{-1}.[51]

The nature of carbon in Ni−N−C@NC was further confirmed by X-ray photoelectron spectroscopy. The high-resolution C 1s spectrum was deconvoluted into four peaks at 283.38, 283.97, 285.09, and 287.5 eV of carbon C=C, C−C, C=N, and C−N bond present in the Ni−N−C@NC catalyst (**Figure 4.2c**).[52] The N 1s XPS was fitted into four peaks of the pyridinic-N, Ni−N, pyrrolic−N, and graphitic−N with corresponding binding energies 397.6, 398.1, 398.5, and 400.0 eV (**Figure 4.2d**). In this study, confirmed the doping of N in the carbon matrix and the formation of Ni−N bond.[46]

The Ni 2p XPS spectrum was fitted into two peaks with Ni $2p_{3/2}$ and Ni $2p_{1/2}$ appeared at 854.4 and 871.8 eV, respectively with at the same position the two metallic Ni(0) peaks observed (**Figure 4.2e**). The peaks located at 858.9 eV are ascribed to Ni^{2+}, which is an indicator of surface oxidation of metallic Ni, and two peaks observed at 862.6 and 879.8 eV of the satellite peaks.[53] The O 1s XPS spectra were deconvoluted into three peaks at 531.0, 531.9, and 533.6 eV corresponding the Ni−O, C−O, and C−OH

bonds (Figure 4.2f).[54]

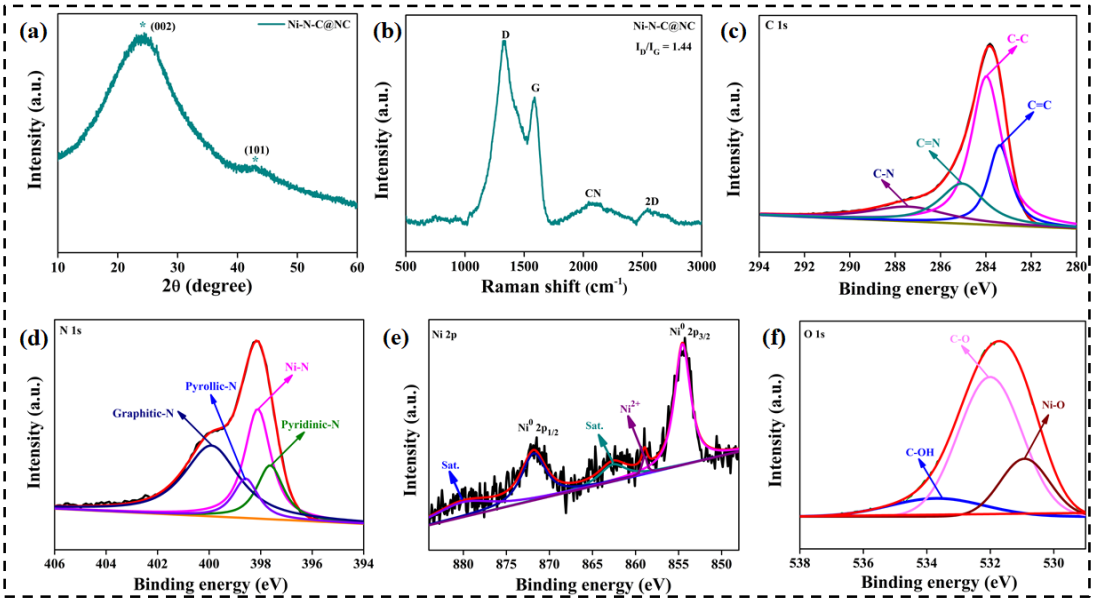

Figure 4.2. (a) The C 1s spectrum of Ni−N−C@NC was deconvoluted into four peaks for C=C, C−C, C=N, and C−N. (b) The N 1s spectrum was fitted into four peaks- corresponding to pyridinic-N, Ni−N, pyrrolic−N, and graphitic nitrogen. (c) Ni 2p XPS was fitted into peaks for Ni(0) and Ni(II) species. The * marked peaks are originated as the satellite peaks of Ni^{2+}. (d) O 1s spectrum of Ni−N−C@NC deconvulated into three peaks for Ni−O, C−O and C−OH.

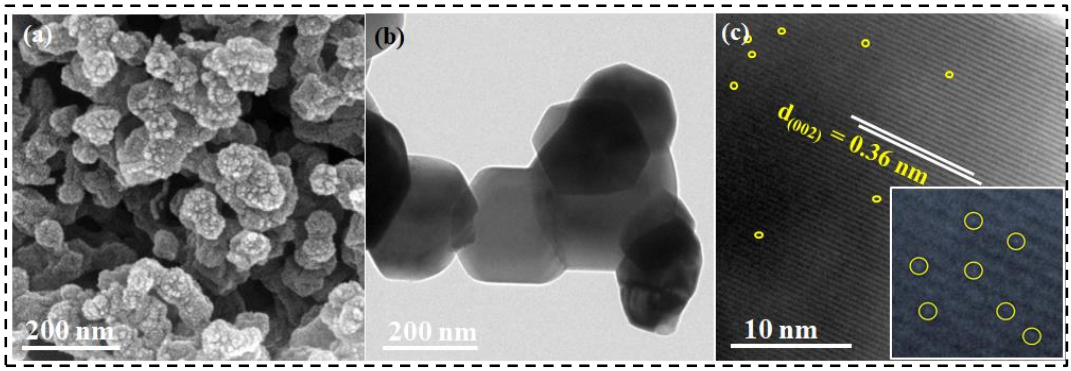

Figure 4.3 (a) FE-SEM image of Ni-−N−C@NC showing the rhombic dodecahedron morphology of the particles. (b) TEM images of Ni−N−C@NC with nanoparticle and the size of the particles was very fine. (c) HR-TEM image showing the inter-planar spacing between the graphene layers is 0.36 nm with (002) plane and inset SAED pattern of the Ni−N−C@NC.

The morphology of the Ni−N−C@NC nanocatalysts was confirmed by the FE-SEM (**Figure 4.3a**). The Ni−N−C@NC catalysts have destroyed rhombic dodecahedron morphology dew to evaporation of Zn from the surface. Further, we have confirmed the morphological features by transmission electron microscopy (TEM) studies (**Figure 4.3b**). The Ni−N−C@NC catalyst showed the nanoparticle nature, but the size of the particle cannot be measured due to its atomic-scale size. The selected area electron diffraction (SAED) pattern of Ni−N−C@NC showed the diffraction rings of the N−doped carbon (NC) corresponding to the crystal planes (002) and (101) (**Figure 4.3c**). The d-spacing of NC was calculated to be 0.36 nm, corresponding to (002) plane of graphene (**Figure 4.3d**).[53] The EDX elemental mapping of the Ni−N−C@NC catalyst was uniformly distributed elements such as Ni, N, and C (**Figure 4.3e-f**).

4.6. Optimization reaction condition

The optimization of the catalytic amidation has been carried out by the reaction of benzaldehyde and piperidine in the presence of Ni−N−C@NC and terminal oxidant tert-butyl hydroperoxide (TBHP). Under mild reaction conditions (60 ^{o}C, dioxan as the solvent), the reaction completed within 4 h to obtain 98% yield of phenyl(piperidine-1-yl) methanone (**4**) (**Table 4.1, entry 1**). In the absence of the catalyst, only TBHP can produce 45% yield of **4** while without the use of TBHP, Ni−N−C@NC produced yield (62%) under similar reaction conditions (**Table 4.1, entries 7-8**). The catalysts prepared at different pyrolysis temperatures (700-900 ^{o}C) showed a varying yield (82-98%) (**Table 4.1, entries 1-3**). The importance of Ni-N coordination was realized when a very low yield of **4** was obtained with catalyst Ni@C under similar reaction conditions (**Table S1, entries 4-6**). The terminal oxidant has also a significant effect on the yield

of the reaction and the best yield was obtained with TBHP (**Table 4.1, entries 9-11**). The different amounts of Ni−N−C@NC catalyst also played an important role in the

Table 4.1. Optimization table for amidation reaction with aldehyde and amine.

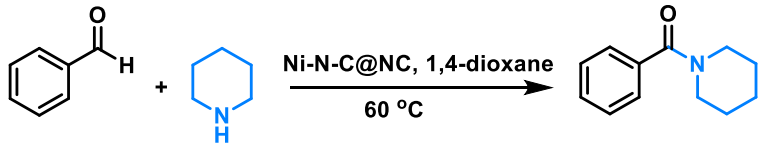

Benzaldehyde **Pipredine** **4**

Entry	Catalyst	Solvent	Oxidant	Temp. (°C)	Time (h)	Yield (%)
Variation in catalysts						
1.	Ni−N−C@NC	Dioxane	TBHP (0.35 eq)	60	4	98
2.	Ni−N−C@NC-AC-1	Dioxane	TBHP (0.35 eq)	60	4	86
3.	Ni−N−C@NC-AC-2	Dioxane	TBHP (0.35 eq)	60	4	82
4.	Ni@C	Dioxane	TBHP (0.35 eq)	60	4	75
5.	Ni-ZIF-8	Dioxane	TBHP (0.35 eq)	60	4	38
6.	$Ni(NO_3)_2.6H_2O$	Dioxane	TBHP (0.35 eq)	60	4	36
Variation of oxidant						
7.	Ni−N−C@NC	Dioxane	Air	60	4	62
8.	…….	Dioxane	TBHP (0.35 eq)	60	4	45
9.	Ni−N−C@NC	Dioxane	TBHP (0.35 eq)	60	4	98
10.	Ni−N−C@NC	Dioxane	H_2O_2 (1 eq)	60	4	82
11.	Ni−N−C@NC	Dioxane	O_2	60	10	70
Variation of the amount of catalyst						
12.	Ni−N−C@NC (1mg)	Dioxane	TBHP (0.35 eq)	60	4	76
13.	Ni−N−C@NC (2 mg)	Dioxane	TBHP (0.35 eq)	60	4	78
14.	Ni−N−C@NC (4 mg)	Dioxane	TBHP (0.35 eq)	60	4	85
15.	Ni−N−C@NC (5 mg)	Dioxane	TBHP (0.35 eq)	60	4	98
16.	Ni−N−C@NC (10 mg)	Dioxane	TBHP (0.35 eq)	60	4	98
Variation of solvent						
17.	Ni−N−C@NC	DMF	TBHP (0.35 eq)	60	4	55
18.	Ni−N−C@NC	THF	TBHP (0.35 eq)	60	4	83
19.	Ni−N−C@NC	H_2O	TBHP (0.35 eq)	60	4	31
20.	Ni−N−C@NC	CH_3CN	TBHP (0.35 eq)	60	4	80
21.	Ni−N−C@NC	Methanol	TBHP (0.35 eq)	60	4	35
22.	Ni−N−C@NC	Dioxane	TBHP (0.35 eq)	60	4	98
Variation of temperature						
23.	Ni−N−C@NC	Dioxane	TBHP (0.35 eq)	50	4	81
24.	Ni−N−C@NC	Dioxane	TBHP (0.35 eq)	60	4	98
25.	Ni−N−C@NC	Dioxane	TBHP (0.35 eq)	70	4	97

Reaction condition: Benzaldehyde (1 mmol), piperidine (1 mmol), catalyst (5 mg), TBHP (0.35 eq., 70% in water), dioxane (2 mL), 60 °C, and 4 h.

product formation. We observed that 5 mg Ni−N−C@NC produced the best result (**Table 4.1, entries 12-16**). Further, the amidation reaction was carried out in different solvents and the best result was obtained in 1,4-dioxan (**Table 4.1, entries 17-22**). Also, we have evaluated the effect of different temperatures on the amide bond formation reactions. The yield of the amide was increased from 81% to 98% when the temperature of the reaction was varied from 50 ºC to 60 ºC and at 70 ºC no significant change in the rate of the reaction was observed. (**Table 4.1, entries 23-25**).

4.7. Scope of aldehydes

A wide variety of benzaldehydes were studied under optimal conditions to react with pipyridine forming a series of amides (**4a-4l, Scheme 1 and Table 4.2**). Under the optimized reaction conditions, the isolated yield of **4a-4l** varied from 64-98%. The electronic properties of the substituents in the benzaldehyde play a significant role to

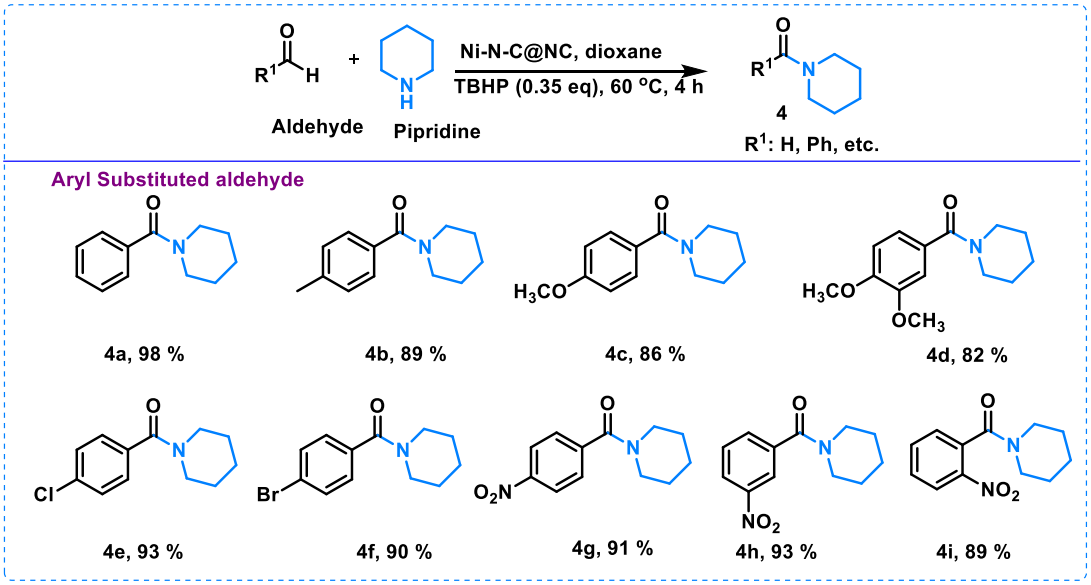

Scheme 4.2: Ni−N−C@NC catalyzed amidation reaction of substituted benzaldehydes with pipyridine. Reaction conditions: Benzaldehyde (1 mmol), piperidine (1 mmol), catalyst (5 mg), TBHP (0.35 eq), dioxane (2 mL), 60 ºC, and 4 h.

control the yield of the amide formation. The electron-donating group such as methyl and methoxy group in the *para*-position of benzaldehydes decreases the yield of the products (**Scheme 4.2, 4a-4c**) and the steric crowding is also affect the product yield (4d). The electron-withdrawing group in the para-position of benzaldehydes comparatively produced higher yields of amides than that of electron donating groups (**Scheme 4.2, 3e-3f, Table 4.2**).

As the nitro-substituted amides are useful intermediates in the pharmaceutical industries, the reactions of nitro benzaldehydes and pipyridine have been carried out with Ni−N−C@NC under optimized conditions. The strong electron-withdrawing substituents -NO_2 at *ortho*-, *meta*-, and *para*- positions of benzaldehyde produced a slight variation in the yields of the amides when reacted with pipyridine (**Scheme 4.2, 3g-3i, Table 4.2**).

4.8. Scope of amines

The scopes of different primary and secondary amines for the amidation reaction have been studied with substituted aldehydes. These amides are highly important in the chemical and pharmaceutical industries as well as for the formation of peptide bonds. The reaction of primary amines and benzaldehyde to form amide is extremely challenging because of some byproduct is also formed during the reaction. The variation of primary and secondary aliphatic and aromatic amines with benzaldehyde derivatives formed amides with 64-89% yield. The benzylamine substrate was taken with aldehyde derivative to slightly decrease the yield of the amide (**Scheme 4.2, 4aa, 4ac, Table 4.2**). The steric crowding also decreased the yield of the amide product (**Scheme 4.3, 4ab, 4ad Table 4.2**). When we move from a six-membered cyclic amine to a five-membered one, product yield decreased due to the dominating ring strain (**Scheme 4.2, 4ae-4ai,**

Table 4.2). The increasing steric hindrance on amine derivatives decreases the yield of products (4aj). The sterically demanding N-Methyl benzylamine was transformed into amides with 88% yield.(Scheme 4.2, 4ak-4al, Table 4.2).

The aniline-based amide products are also useful in the chemical industries. In the aniline-derived amide bond formation reaction product yield (82-75%) decreases due to

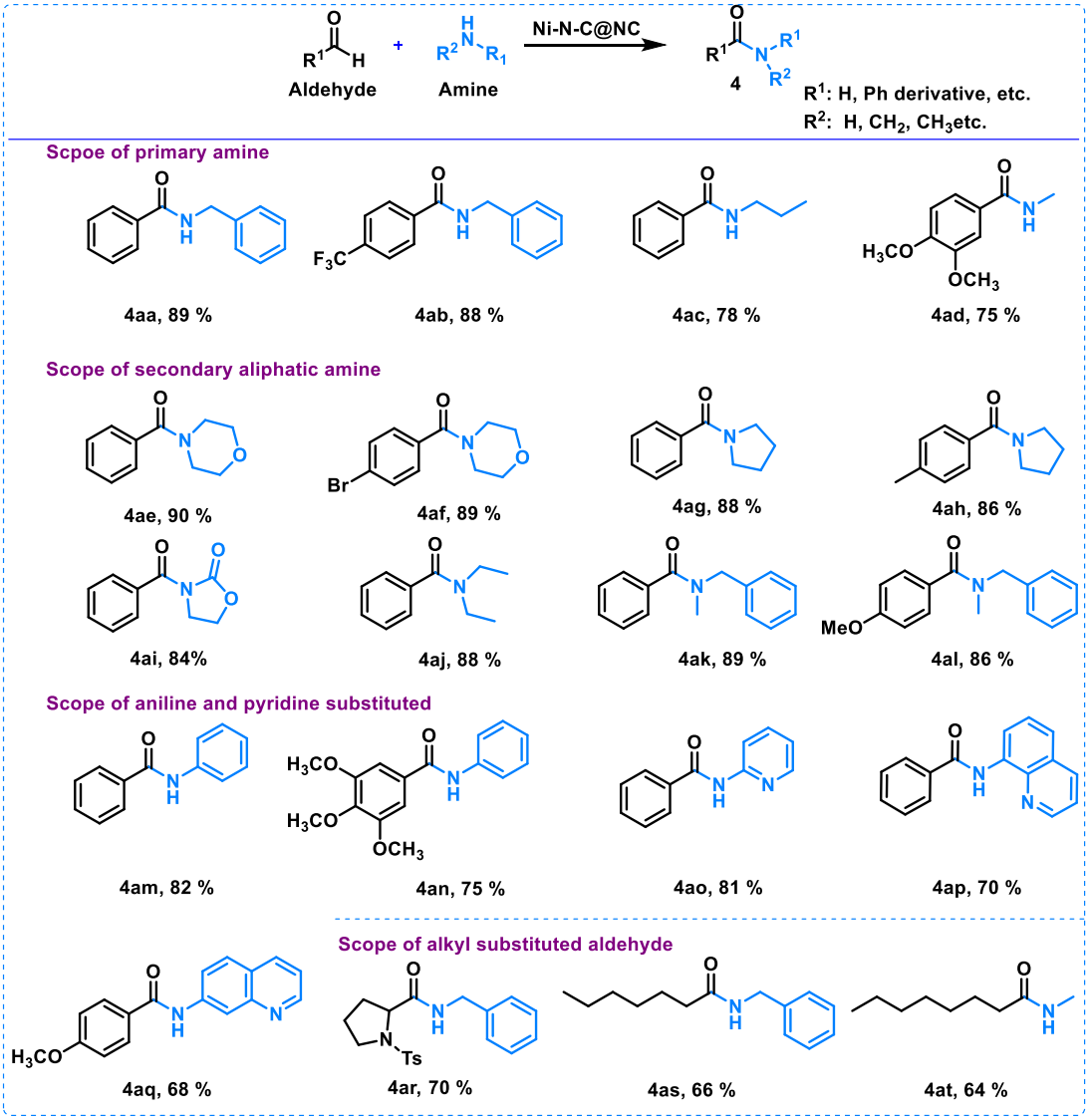

Scheme 4.3: Amidation reaction with various amines and aldehyde with Ni−N−C@NC catalyst. Reaction condition: Aldehyde (1 mmol), amine (1 mmol), catalyst (5 mg), TBHP (0.35 eq), dioxane (2 mL), 60 °C, and 4 h.

steric hindrance (**Scheme 4.2, 4am-4an, Table 4.2**). The pyridine-derived amide provides the best yield (81%), and when steric crowding increase, the yield of the compound is also important in the pharmaceutical and other fields. The 2-aminopyridine product decrease (**Scheme 4.3, 4ao-4aq, Table 4.2**). It is worth mention the aliphatic aldehyde and benzylic amine afford moderate yield of 64-70% (**Scheme 4.3, 4ar-4as, Table 4.2.**). The aliphatic primary amine obtained a moderate yield (64%) with the aliphatic aldehyde (**4at**). The region behind the moderate yield is the steric hindrance of the substrate and aliphatic primary amine also not provided a better yield of the amide products. Therefore, the most of the primary and secondary amine derivative amide products are very useful in the amino acid (peptide linkage bond), chemical industries, and pharmaceutical industries.

4.9. Reaction mechanism of amide bond formation

We have proposed the reaction mechanism for the oxidative amide bond formation reaction with the Ni−N−C@NC. The reaction proceeds through a radical mechanism. First, the TBHP was reacted with the Ni−N−C@NC catalyst to activate the TBHP and its produced $^{t}BuO^{\bullet}$ and $^{\bullet}OH$ radicals through the homolytic cleavage path. The presence of amine and benzaldehyde substrates on the catalyst surface promotes the generation of corresponding radicals through interaction with $tBuO^{\bullet}$ and $^{\bullet}OH$ radicals. Therefore, the acyl and amine radicals undergo a radical-radical coupling process, finally producing an amide bond (**Figure 4.3a**).[55]

The catalytic reusability is an important factor for the environmental and economic point of view. The catalytic activity of the Ni-N-C@NC catalyst was investigated by the multiple experimental cycles repeated under the optimized reaction condition of the

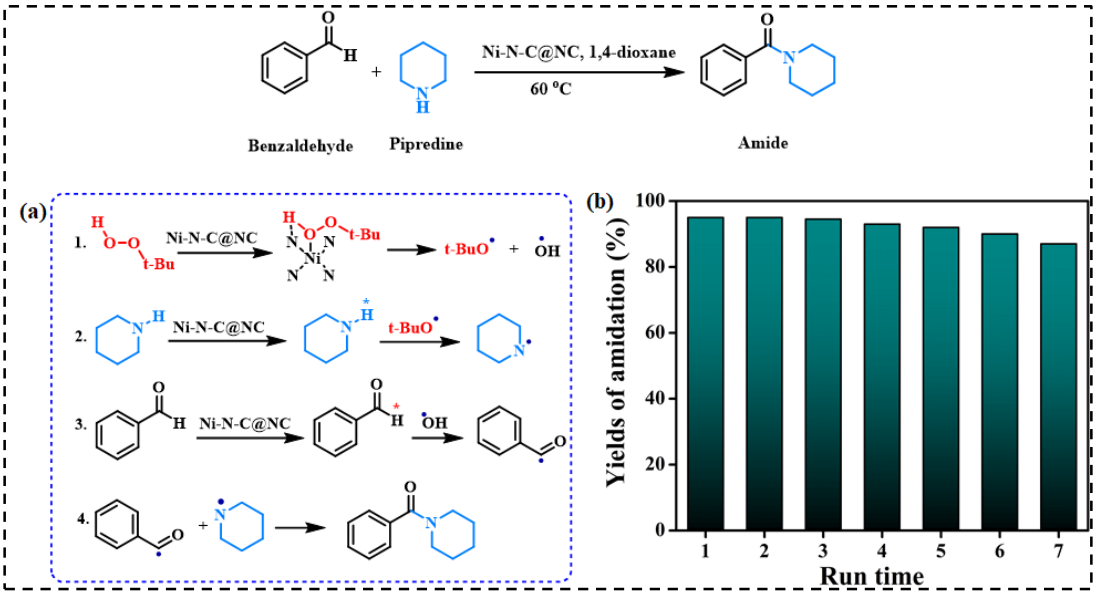

Figure 4.4: (a) Reaction mechanism of the amide reaction with the Ni−N−C@NC. (b) Recyclability graph of the Ni−N−C@NC nanocatalysts for the amide bond formation reactions.

amide reaction of a substituted aldehyde with piperidine (**Figure 4.4b**). After the completion of each reaction, the catalyst was separated from the reaction mixture by centrifugation, washed with water, methanol, and ethyl acetate several times, and dried hot air oven and then reused for next cycle. The Ni−N−C@NC catalyst was recyclable for seven times without loss of catalytic activity.

4.10. Conclusion

We have demonstrated the MOF-derived Ni−N−C@NC nanocatalysts from the pyrolysis of precursor materials of the Ni-ZIF-8. The Ni−N−C@NC catalysts have provided excellent activity for the amidation reaction of aldehyde and amine with oxidant. The low loading of Ni (0.25 atomic%) in Ni−N−C@NC offered excellent turnover number for the amide bond formation reaction. The Ni−N coordination provides strong electronic structure modulation to improve the catalytic activity of the amide bond formation reactions. Moreover,

the Ni−N−C@NC catalyst shows remarkable stability for the amide bond formation reaction with various substitutions.

Table 4.2. Characterization of the various products of the ^{1}H NMR and ^{13}C NMR

4a: phenyl(piperidine-1-yl) methanone 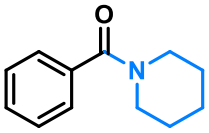	**^{1}H NMR** (500 MHz, $CDCl_3$) δ 7.41 (m, *J* = 3.9 Hz, 5H), 3.73 (s, 2H), 3.36 (s, 2H), 1.61 (d, *J* = 79.3 Hz, 6H). **^{13}C NMR** (125 MHz, $CDCl_3$) δ 170.41, 136.45, 129.37, 128.40, 126.81, 48.75, 43.19, 26.07, 25.60, 24.59. Yield of product: 185.5 mg, 98%.
4b: piperidine-1-yl(p-tolyl) methanone 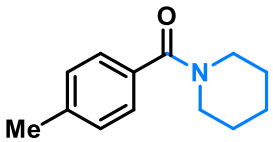	**^{1}H NMR** (500 MHz, $CDCl_3$) δ 7.29 (d, *J* = 8.0 Hz, 2H), 7.19 (d, *J* = 7.8 Hz, 2H), 3.70 (s, 2H), 3.36 (s, 2H), 2.37 (s, 3H), 1.70 – 1.47 (m, 6H). **^{13}C NMR** (125 MHz, $CDCl_3$) δ 170.59, 139.45, 133.48, 128.98, 126.92, 24.61, 21.34. Yield of product: 90 mg, 89%.
4c: (4-methoxyphenyl) (piperidine-1-yl)methanone 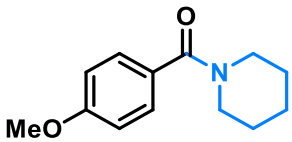	**^{1}H NMR** (500 MHz, $CDCl_3$) δ 7.37 (d, 2H), 6.90 (d, 2H), 3.83 (s, 3H), 3.56 (dd, 4H), 1.64 (d, *J* = 43.8 Hz, 6H). **^{13}C NMR** (125 MHz, $CDCl_3$) δ 170.38, 160.56, 128.88, 128.63, 113.67, 55.35, 24.68. Yield of product: 188 mg, 86%.
4d: (3,4-dimethoxyphenyl) (piperidine-1-yl)methanone 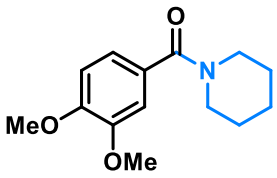	**^{1}H NMR** (600 MHz, $CDCl_3$) δ 6.98 – 6.94 (m, 2H), 6.85 (d, 1H), 3.89 (d, 6H), 3.55 (t, 4H), 1.63 (m, 6H). **^{13}C NMR** (150 MHz, $CDCl_3$) δ 170.24, 150.00, 148.84, 128.69, 119.78, 110.68, 110.47, 55.92, 24.60. Yield of product: 102.2 mg, 82%.
4e: (4-chlorophenyl) (piperidine-1-yl) methanone 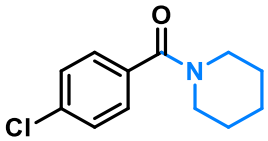	**^{1}H NMR** (CDCl3, 500 MHz): *δ* 7.36-7.42 (m, 4H), 3.71 (br s, 2H), 3.34 (br s, 2H), 1.53-1.70 (m, 6H); **^{13}C NMR** (126 MHz, $CDCl_3$): *δ* 169.24, 135.41, 134.86, 128.69, 128.38, 48.77, 43.24, 26.55, 25.58, 24.54. Yield of product: 104 mg, 93%.
4f: (4-bromophenyl) (piperidine-1-yl) methanone 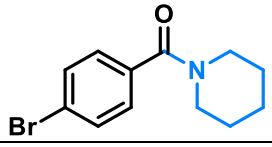	**^{1}H NMR** (500 MHz, $CDCl_3$) δ 7.54 (d, *J* = 8.3 Hz, 2H), 7.37 – 7.22 (m, 2H), 3.70 (br, s, 2H), 3.34 (br, s, 2H), 1.78 – 1.49 (m, 6H). **^{13}C NMR** (126 MHz, $CDCl_3$) δ 169.31, 135.26, 131.64, 128.59, 123.65, 48.80, 43.30, 26.01, 24.52. Yield of product: 120.7 mg, 90%.
4g: (3-nitrophenyl) (piperidine-1-yl) methanone	**^{1}H NMR** (500 MHz, $CDCl_3$) δ 8.27 (d, *J* = 8.6 Hz, 1H), 7.56 (d, *J* = 8.7 Hz, 1H), 3.74 (s, 1H), 3.29 (s, 1H), 1.71 (s, 2H), 1.54 (s, 1H).

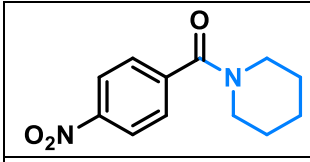	**^{13}C NMR** (125 MHz, $CDCl_3$) δ 167.93, 148.21, 142.68, 127.81, 123.85, 48.66, 43.23, 26.51, 25.50, 24.39. Yield of product: 162 mg, 92%.
4h: (3-nitrophenyl) (piperidine-1-yl) methanone 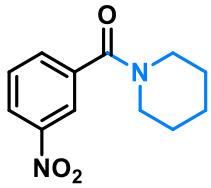	**^{1}H NMR** (500 MHz, $CDCl_3$) δ 8.28 (d, *J* = 7.1 Hz, 2H), 7.75 (d, *J* = 7.6 Hz, 1H), 7.62 (t, *J* = 7.4 Hz, 1H), 3.74 (br s, 2H), 3.35 (br, s, 2H), 1.64 (m, *J* = 76.7 Hz, 6H). **^{13}C NMR** (125 MHz, $CDCl_3$) δ 167.60, 148.07, 138.08, 132.90, 129.73, 124.22, 122.05, 48.84, 43.37, 26.52, 25.51, 24.41. Yield of product: 178 mg, 93%.
4i: (2-nitrophenyl) (piperidine-1-yl) methanone 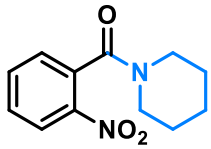	**^{1}H NMR** (500 MHz, $CDCl_3$) δ 8.17 (d, *J* = 8.3 Hz, 1H), 7.70 (t, *J* = 7.5 Hz, 1H), 7.55 (t, *J* = 7.9 Hz, 1H), 7.39 (d, *J* = 1.3 Hz, 1H), 3.76 (s, 2H), 3.16 (t, *J* = 5.6 Hz, 2H), 1.77 – 1.44 (m, 6H). **^{13}C NMR** (125 MHz, $CDCl_3$) δ 166.24, 145.19, 134.40, 133.36, 129.56, 127.96, 124.69, 47.92, 42.70, 25.76, 25.08, 24.41. Yield of product: 190 mg, 90%.
4aa: N-benzylbenzamide 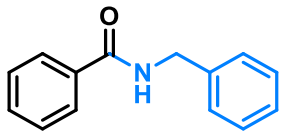	**^{1}H NMR** (500 MHz, $CDCl_3$) δ 7.82 (d, *J* = 7.5 Hz, 2H), 7.53 – 7.48 (m, 1H), 7.43 (d, *J* = 7.5 Hz, 2H), 7.40 – 7.29 (m, 5H), 6.78 (s, 1H), 4.65 (s, 2H). **^{13}C NMR** (126 MHz, $CDCl_3$) δ 167.51, 138.31, 134.43, 131.54, 128.77, 128.58, 127.89, 127.57, 127.06, 44.11. Yield of product: 96 mg, 89 %.
4ab: N-propylbenzamide 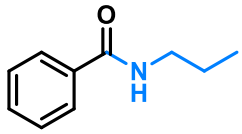	**^{1}H NMR** (500 MHz, $CDCl_3$) δ 7.83 – 7.75 (m, 2H), 7.44 (d, *J* = 29.8 Hz, 3H), 6.56 (s, 1H), 3.48 – 3.35 (m, 2H), 1.72 – 1.57 (m, 2H), 1.04 – 0.92 (m, 3H). **^{13}C NMR** (125 MHz, $CDCl_3$) δ 167.67, 134.89, 131.24, 128.47, 126.90, 41.77, 22.91, 11.44. Yield of product: 127.1 mg, 78 %.
4ad: 3,4-dimethoxy-N-methylbenzamide 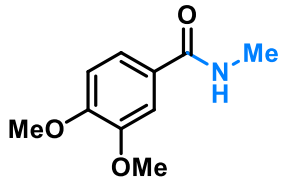	**^{1}H NMR** (500 MHz, $CDCl_3$) δ 10.27 (s, 1H), 7.67 (s, 1H), 7.41 (d, *J* = 24.1 Hz, 1H), 7.07 (s, 1H), 3.84 (d, *J* = 25.3 Hz, 6H), 2.96 (s, 3H). **^{13}C NMR** (125 MHz, $CDCl_3$) δ 168.35, 151.60, 148.81, 127.20, 121.83, 119.86, 110.53, 55.94, 26.83. Yield of product: 76.9 mg, 78 %.
4ae: phenyl(morpholine) methanone 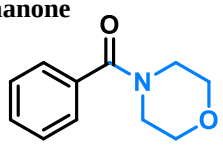	**^{1}H NMR** (600 MHz, $CDCl_3$) δ 7.46 – 7.39 (m, 5H), 3.81 – 3.42 (t, 8H). **^{13}C NMR** (151 MHz, $CDCl_3$) δ 163.46, 128.26, 122.89, 121.55, 120.07, 59.87, 41.24. Yield: 137.6 mg, 90%.
4af:(4-bromophenyl) (morpholine) methanone	**^{1}H NMR** (500 MHz, $CDCl_3$) δ 7.40 (d, *J* = 8.8 Hz, 2H), 6.93 (d, *J* = 6.5 Hz, 2H), 3.84 (dd, *J* = 2.8, 1.1 Hz, 2H), 3.71 (s, 2H).

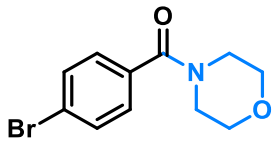	**^{13}C NMR** (125 MHz, $CDCl_3$) δ 170.46, 160.93, 129.21, 127.32, 113.81, 66.92, 55.36. Yield: 122.2 mg, 90%.
4ag: phenyl(pyrrolidin-1-yl) methanone 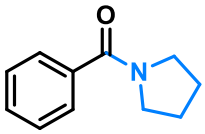	**^{1}H NMR** (600 MHz, $CDCl_3$) δ 7.51 (d, 2H), 7.40 (t, 3H), 3.65 (t, 2H), 3.42 (t, 2H), 1.95 (m, 2H), 1.87 (m, *J* = 6.7 Hz, 2H). **^{13}C NMR** (150 MHz, $CDCl_3$) δ 169.81, 137.10, 129.81, 128.24, 127.06, 49.63, 46.20, 26.35, 24.43. Yield of product: 123.5 mg, 88%.
4ah: pyrrolidin-1-yl(p-tolyl)methanone 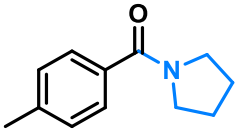	**^{1}H NMR** (500 MHz, $CDCl_3$) δ 7.43 (d, *J* = 8.1 Hz, 2H), 7.19 (d, *J* = 8.2 Hz, 2H), 3.64 (t, *J* = 6.8 Hz, 2H), 3.44 (t, *J* = 6.5 Hz, 2H), 2.37 (s, 3H), 1.97 – 1.91 (m, 2H), 1.89 – 1.82 (m, 2H). **^{13}C NMR** (125 MHz, $CDCl_3$) δ 169.84, 139.87, 134.31, 128.80, 127.21, 49.63, 46.18, 26.40, 24.44, 21.36. Yield of product: 166.0 mg, 86%.
4ai: 3-benzoyloxazolidin-2-one 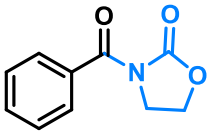	**^{1}H NMR** (500 MHz, $CDCl_3$) δ 7.68 (d, *J* = 7.9 Hz, 2H), 7.57 (t, *J* = 7.4 Hz, 1H), 7.45 (t, *J* = 7.7 Hz, 2H), 4.49 (t, *J* = 7.8 Hz, 2H), 4.18 (t, *J* = 7.8 Hz, 2H). **^{13}C NMR** (126 MHz, $CDCl_3$) δ 169.81, 153.24, 132.66, 132.41, 129.09, 127.89, 62.27, 43.72. Yield of product: 163.0 mg, 83%.
4aj: N,N-diethylbenzamide 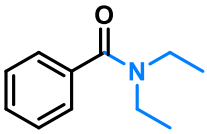	**^{1}H NMR** (500 MHz, $CDCl_3$) δ 7.42 – 7.35 (m, 5H), 3.42 (d, *J* = 147.9 Hz, 4H), 1.19 (d, *J* = 71.1 Hz, 6H). **^{13}C NMR** (126 MHz, $CDCl_3$) δ 171.30, 137.32, 129.07, 128.38, 126.28, 43.26, 39.23, 14.23, 12.90. Yield of product: 155.7 mg, 88%.
4ak: N-benzyl -N-methylbenzamide 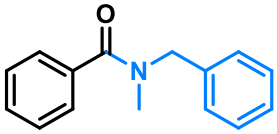	**^{1}H NMR** (600 MHz, $CDCl_3$) δ 7.47 (d, 2H), 7.38 (m, 6H), 7.32 (d, 1H), 7.19 (d, 1H), 4.79 (s, 2H), 3.06 (s, 3H). **^{13}C NMR** ($CDCl_3$, 150 MHz): *δ* 160.51, 136.47, 130.24, 129.01, 128.57, 128.37, 128.15, 127.23, 126.41, 55.16, 35.14. Yield of product: 100.3 mg, 89%.
4al: N-benzyl-4-methoxy-N-methylbenzamide 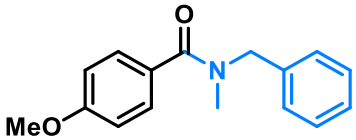	**^{1}H NMR** (500 MHz, $CDCl_3$) δ 7.46 (d, *J* = 8.8 Hz, 2H), 7.38 (t, *J* = 7.4 Hz, 3H), 7.31 (t, *J* = 7.5 Hz, 2H), 6.91 (d, *J* = 6.9 Hz, 2H), 4.66 (s, 2H), 3.83 (s, 3H), 2.98 (s, 3H). **^{13}C NMR** (126 MHz, $CDCl_3$) δ 160.73, 137.08, 129.63, 128.99, 128.45, 128.00, 127.32, 126.93, 113.69, 55.33, 50.81, 37.07. Yield of product: 112.2 mg, 88%.

4am: N-phenylbenzamide 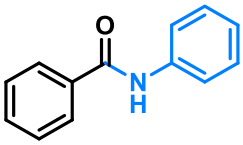	**^{1}H NMR** (500 MHz, $CDCl_3$) δ 7.91 (s, 1H), 7.85 (d, 2H), 7.40-7.45 (m, 5H), 7.17 (t, 1H), 7.09 (d, 2H). **^{13}C NMR** (126 MHz, $CDCl_3$) δ 166.51, 137.32, 136.80, 132.13, 130.18, 129.90, 128.12, 124.30, 122.53, 60.95, 56.36. Yield of product: 80.9 mg, 82%.
4an: **3,4,5-trimethoxy-N-phenylbenzamide** 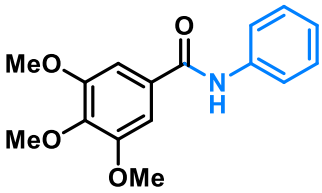	**^{1}H NMR** (500 MHz, $CDCl_3$) δ 7.95 (s, 1H), 7.65 (d, 2H), 7.37 (dd, 2H), 7.17 (dd, 1H), 7.09 (s, 2H), 3.90 (s, 9H). **^{13}C NMR** (126 MHz, $CDCl_3$) δ 165.65, 153.32, 141.20, 137.93, 130.48, 129.09, 124.61, 120.30, 104.53, 60.95, 56.36. Yield of product: 54.9 mg, 75%.
4ao: N-(pyridine-2-yl)-benzamide 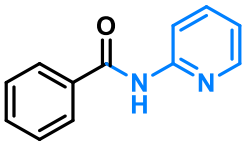	**^{1}H NMR** (600 MHz, $CDCl_3$) δ 9.33 (s, 1H), 8.45 (d, 1H), 8.23 (d, 1H), 7.98 (d, *J* = 7.4 Hz, 2H), 7.78 (t, *J* = 8.8 Hz, 1H), 7.58 (t, *J* = 7.4 Hz, 1H), 7.50 (t, *J* = 7.6 Hz, 2H), 7.08 (dd, *J* = 7.2, 5.0 Hz, 1H). **^{13}C NMR** (151 MHz, $CDCl_3$) δ 166.08 (s), 151.76 (s), 147.47 (s), 138.75 (s), 134.28 (s), 132.23 (s), 128.77 (s), 127.44 (s), 119.88 (s), 114.57 (s). Yield of product: 80 mg, 81%.
4ap: 3p. 1-phenyl-2-(quinolin-7-yl)ethan-1-one 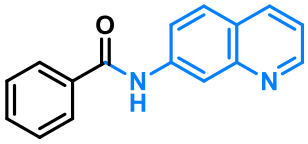	**^{1}H NMR** (500 MHz, $CDCl_3$) δ 10.77 (s, 2H), 8.97 (d, *J* = 7.6 Hz, 2H), 8.86 (s, 2H), 8.19 (t, *J* = 7.7 Hz, 2H), 8.12 (d, *J* = 7.3 Hz, 4H), 7.58 (d, *J* = 9.5 Hz, 11H), 7.48 (dd, *J* = 7.5, 4.7 Hz, 2H). **^{13}C NMR** (125 MHz, $CDCl_3$) δ 165.46, 148.30, 138.82, 136.39, 135.21, 134.63, 131.84, 128.81, 128.02, 127.48, 127.31, 121.69, 116.56. Yield of product: 60.5 mg, 70%.
4aq: 4-methoxy-N-(quinolone-8-yl) benzamide 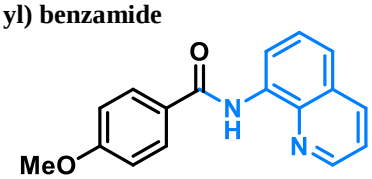	**^{1}H NMR** (500 MHz, $CDCl_3$) δ 10.70 (s, 1H), 8.95 (d, *J* = 7.6 Hz, 1H), 8.87 (d, 1H), 8.19 (d, 1H), 8.08 (d, 2H), 7.61 (t, *J* = 7.9 Hz, 1H), 7.54 (d, 1H), 7.49 (dd, 1H), 7.06 (d, 2H), 3.91 (s, 3H). **^{13}C NMR** (125 MHz, $CDCl_3$) δ 165.03, 162.54, 148.22, 138.81, 136.39, 134.80, 132.83, 129.19, 128.03, 127.52, 121.64, 121.40, 116.39, 114.01, 55.48. Yield of product: 47.2 mg, 68%.
4ar: N-benzyl-2-tosylcyclopentane-1-carboxamide 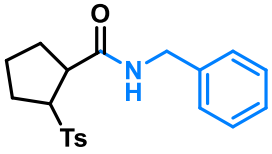	**^{1}H NMR** (500 MHz, $CDCl_3$) δ 7.74 (d, *J* = 7.7 Hz, 4H), 7.38 – 7.29 (m, 14H), 4.52 (d, *J* = 5.6 Hz, 4H), 4.39 (s, 1H), 4.16 (d, *J* = 7.6 Hz, 2H), 3.60 – 3.49 (m, 2H), 3.19 (d, *J* = 6.0 Hz, 2H), 2.47 (s, 6H), 2.23 (s, 2H), 1.75 (t, *J* = 12.6 Hz, 2H), 1.63 (d, *J* = 7.5 Hz, 4H). **^{13}C NMR** (125 MHz, $CDCl_3$) δ 171.22, 144.48, 137.96, 132.73, 130.02, 128.72, 127.90, 127.46, 62.69, 49.95, 43.58, 30.18, 24.42, 21.59. Yield: 63.47 mg, 69%.

4as: N-benzylheptanamide 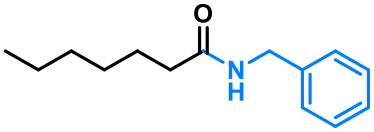	**^{1}H NMR** (500 MHz, $CDCl_3$) δ 8.20 – 8.19 (m, 1H), 7.34 – 7.31 (m, 2H), 7.28 (d, *J* = 6.8 Hz, 3H), 4.44 (s, 2H), 2.23 – 2.20 (m, 2H), 1.68 – 1.64 (m, 2H), 1.41 – 1.24 (m, 6H), 0.90 (d, *J* = 7.0 Hz, 3H). **^{13}C NMR** (126 MHz, $CDCl_3$) δ 173.07, 138.56, 128.65, 127.80, 127.40, 43.52, 39.14, 36.73, 31.48, 25.46, 22.39, 13.92. Yield: 72.2 mg, 66%.
4at: N-methyloctanamide 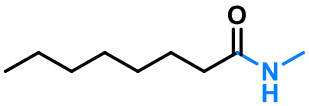	**^{1}H NMR** (500 MHz, $CDCl_3$) δ 5.96 (s, 1H), 2.78 (d, *J* = 4.8 Hz, 3H), 2.19 – 2.12 (m, 2H), 1.64 – 1.56 (m, 2H), 1.31 – 1.22 (m, 8H), 0.86 (t, *J* = 6.5 Hz, 3H). **^{13}C NMR** (125 MHz, $CDCl_3$) δ 174.04, 36.65, 31.67, 29.28, 29.00, 26.19, 25.80, 22.57, 14.02. Yield: 100.8 mg, 64%.

4.11. Spectral data of few products

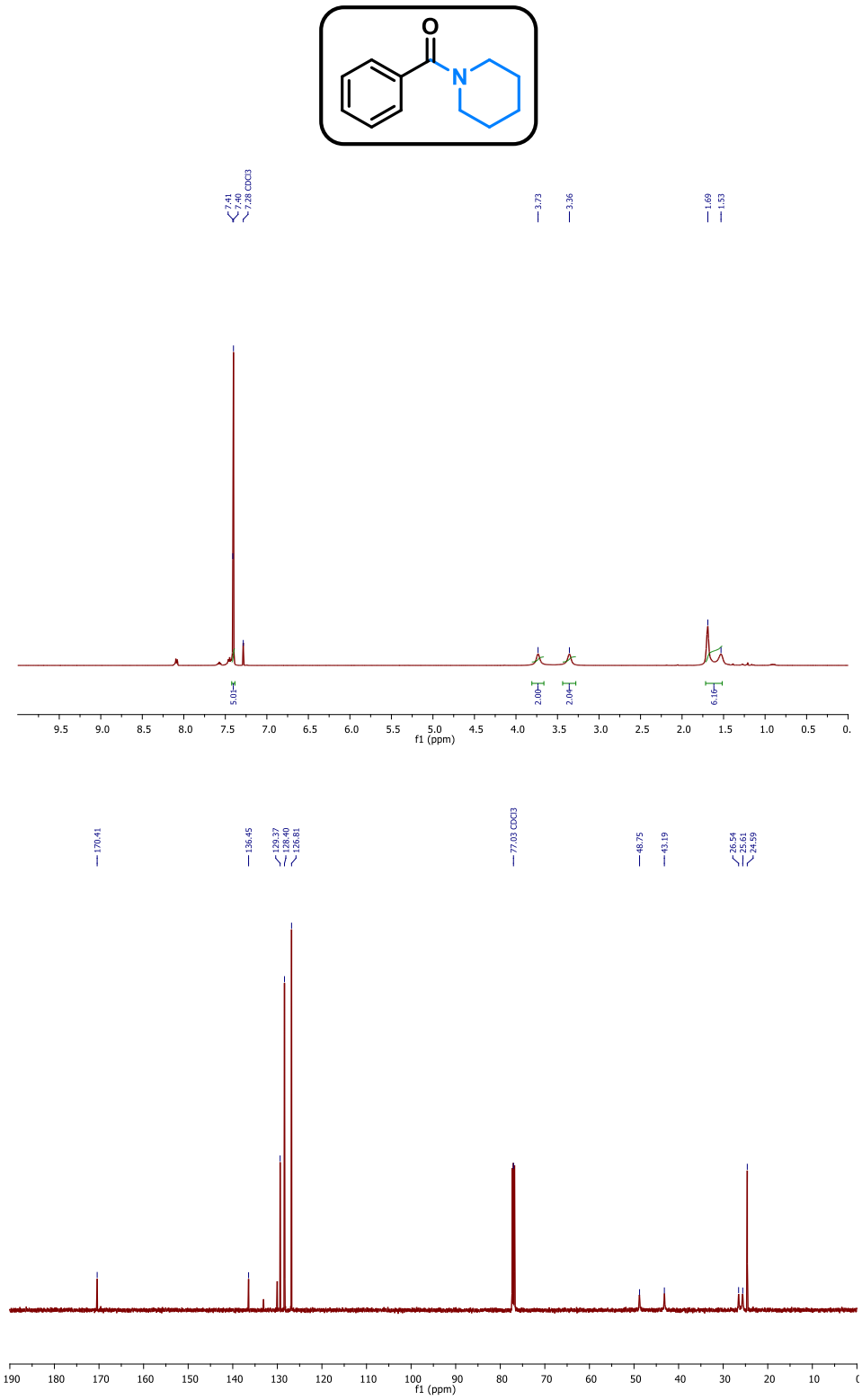

Figure 4.5. ^{1}H NMR ^{13}C NMR spectra of compound **4a** in $CDCl_3$.

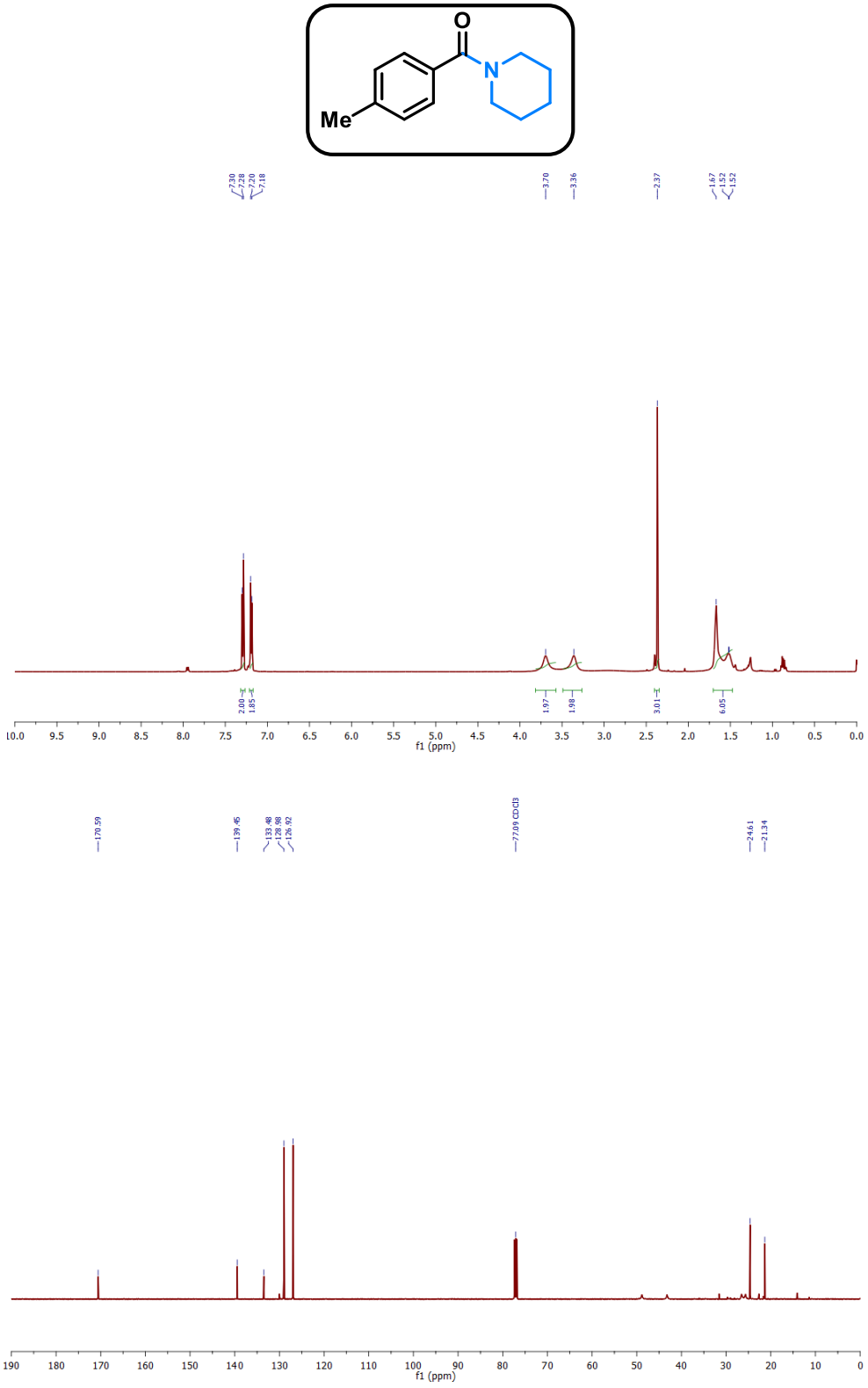

Figure 4.6. ^{1}H NMR and ^{13}C NMR spectra of compound **4b** in $CDCl_3$.

4.12. Reference

[1] Y. Ning, S. Wang, M. Li, J. Han, C. Zhu, J. Xie, *Nat. Commun.* **2021**, *12*, 1–9.

[2] R. M. De Figueiredo, J. S. Suppo, J. M. Campagne, *Chem. Rev.* **2016**, *116*, 12029–12122.

[3] W. Muramatsu, C. Manthena, E. Nakashima, H. Yamamoto, *ACS Catal.* **2020**, *10*, 9594–9603.

[4] J. Gao, R. Ma, F. Poovan, L. Zhang, H. Atia, N. V. Kalevaru, W. Sun, S. Wohlrab, D. A. Chusov, N. Wang, R. V. Jagadeesh, M. Beller, *Nat. Commun.* **2023**, *14*, 1–13.

[5] K. Michigami, T. Sakaguchi, Y. Takemoto, *ACS Catal.* **2020**, *10*, 683–688.

[6] L. Bering, E. J. Craven, S. A. Sowerby Thomas, S. A. Shepherd, J. Micklefield, *Nat. Commun.* **2022**, *13*, 1–10.

[7] S. C. Ghosh, J. S. Y. Ngiam, A. M. Seayad, D. T. Tuan, C. L. L. Chai, A. Chen, *J. Org. Chem.* **2012**, *77*, 8007–8015.

[8] A. Taussat, R. M. de Figueiredo, J. M. Campagne, *Catalysts* **2023**, *13*, 366.

[9] N. Ismaeel, Z. Zhuo, S. Imran, D. Yuan, Y. Yao, *Dalt. Trans.* **2022**, *51*, 13892–13901.

[10] N. Ambreen, T. Wirth, *European J. Org. Chem.* **2014**, *2014*, 7590–7593.

[11] B. L. Jiang, B. H. Xu, M. L. Wang, Z. X. Li, D. S. Liu, S. J. Zhang, *Asian J. Org. Chem.* **2018**, *7*, 977–983.

[12] W. Shu, M. S. Liu, *ACS Catal.* **2020**, *10*, 12960–12966.

[13] A. S. Santos, A. M. S. Silva, M. M. B. Marques, *European J. Org. Chem.* **2020**, *2020*, 2501–2516.

[14] D. C. Braddock, P. D. Lickiss, B. C. Rowley, D. Pugh, T. Purnomo, G. Santhakumar, S. J. Fussell, *Org. Lett.* **2018**, *20*, 950–953.

[15] K. Wang, Y. Lu, K. Ishihara, *Chem. Commun.* **2018**, *54*, 5410–5413.

[16] S. W. Krabbe, V. S. Chan, T. S. Franczyk, S. Shekhar, J. G. Napolitano, C. A. Presto, J. A. Simanis, *J. Org. Chem.* **2016**, *81*, 10688–10697.

[17] W. J. Yoo, C. J. Li, *J. Am. Chem. Soc.* **2006**, *128*, 13064–13065.

[18] M. Saikia, L. Saikia, *RSC Adv.* **2016**, *6*, 14937–14947.

[19] H. Li, X. Fang, R. Jackstell, H. Neumann, M. Beller, *Chem. Commun.* **2016**, *52*, 7142–7145.

[20] Y. Wang, W. Guo, A. L. Guan, S. Liu, Z. J. Yao, *Inorg. Chem.* **2021**, *60*, 11514–11520.

[21] W. G. Jia, X. D. Li, X. T. Zhi, R. Zhong, *Appl. Organomet. Chem.* **2022**, *36*, 1–11.

[22] M. Todorovic, D. M. Perrin, *Pept. Sci.* **2020**, *112*, e24210.

[23] S. A. Runikhina, O. I. Afanasyev, E. A. Kuchuk, D. S. Perekalin, R. V. Jagadeesh, M. Beller, D. Chusov, *Chem. Sci.* **2023**, 4346–4350.

[24] C. Q. Wang, C. Feng, T. P. Loh, *Asian J. Org. Chem.* **2016**, *5*, 1002–1007.

[25] Z. Wu, K. L. Hull, *Chem. Sci.* **2016**, *7*, 969–975.

[26] N. Devika, S. Ananthalakshmi, N. Raja, G. Gupta, B. Therrien, *J. Organomet. Chem.* **2019**, *886*, 65–70.
[27] C. L. Allen, J. M. J. Williams, *Chem. Soc. Rev.* **2011**, *40*, 3405–3415.
[28] T. Wakikawa, D. Sekine, Y. Murata, Y. Bunno, M. Kojima, Y. Nagashima, K. Tanaka, T. Yoshino, S. Matsunaga, *Angew. Chem. Int. Ed.* **2022**, *61*, e202213659.
[29] S. Ni, W. Zhang, H. Mei, J. Han, Y. Pan, *Org. Lett.* **2017**, *19*, 2536–2539.
[30] P. J. Czerwiński, B. Furman, *Front. Chem.* **2021**, *9*, 1–10.
[31] B. Zhao, Y. Xiao, D. Yuan, C. Lu, Y. Yao, *Dalt. Trans.* **2016**, *45*, 3880–3887.
[32] T. Ben Halima, J. Masson-Makdissi, S. G. Newman, *Angew. Chem. Int. Ed.* **2018**, *130*, 13107–13111.
[33] C. W. Cheung, M. Leendert Ploeger, X. Hu, *Chem. Sci.* **2018**, *9*, 655–659.
[34] R. K. Sharma, A. Sharma, S. Sharma, S. Dutta, *Ind. Eng. Chem. Res.* **2018**, *57*, 3617–3627.
[35] K. Pedrood, S. Bahadorikhalili, V. Lotfi, B. Larijani, M. Mahdavi, Molecular Diversity **2022**, *26*, 1311–1344.
[36] H. Ghafuri, P. Hanifehnejad, A. Rashidizadeh, Z. Tajik, H. Dogari, *Sci. Rep.* **2023**, *13*, 1–14.
[37] K. Hasan, R. G. Joseph, S. P. Patole, *ChemistrySelect* **2022**, *7*, 1840.
[38] K. Yamaguchi, H. Kobayashi, Y. Wang, T. Oishi, Y. Ogasawara, N. Mizuno, *Catal. Sci. Technol.* **2013**, *3*, 318–327.
[39] H. Luo, L. Wang, S. Shang, J. Niu, S. Gao, *Commun. Chem.* **2019**, *2*, 17.
[40] R. Wang, K. Lu, J. Zhang, X. Li, Z. Zheng, *ACS Catal.* **2022**, *12*, 14290–14303.
[41] S. Ma, W. Han, W. Han, F. Dong, Z. Tang, *J. Mater. Chem. A* **2023**, *11*, 3315–3363.
[42] T. Y. Su, G. P. Lu, K. K. Sun, M. Zhang, C. Cai, *Catal. Sci. Technol.* **2022**, *12*, 2106–2121.
[43] H. Konnerth, B. M. Matsagar, S. S. Chen, M. H. G. Prechtl, F. Shieh, K. C. Wu, *Coord. Chem. Rev.* **2020**, *416*, 213319.
[44] H. Luo, S. Tian, H. Liang, H. Wang, S. Gao, W. Dai, *Nat. Commun.* **2023**, *14*, 2981.
[45] A. Baghban, H. Ezedin Nejadian, S. Habibzadeh, F. Zokaee Ashtiani, *Sci. Rep.* **2022**, *13*, 8359.
[46] R. Fajri, P. Wahyuningsih, J. Jofrishal, R. Ediati, *E3S Web Conf.* **2022**, *339*, 8–11.
[47] C. Zhou, R. Zhang, Y. Rong, Y. Yang, X. Jiang, *ACS Appl. Mater. Interfaces* **2023**, *15*, 42585–42593.
[48] S. Zhao, J. Chen, *J. Porous Mater.* **2019**, *26*, 381–387.
[49] Y. Zhang, L. Jiao, W. Yang, C. Xie, H. Jiang, *Angew. Chem. Int. Ed.* **2021**, *133*, 7685–7689.
[50] S. Mahalingam, M. Durai, C. Sengottaiyan, Y.-H. Ahn, *J. Nanosci. Nanotechnol.* **2021**,

21, 3183–3191.

[51] G. M. Shi, S. H. Lv, X. Bin Cheng, X. L. Wang, S. T. Li, *J. Mater. Sci. Mater. Electron.* **2018**, *29*, 17483–17492.

[52] Z. Zhu, Z. Li, J. Wang, R. Li, H. Chen, Y. Li, J. S. Chen, R. Wu, Z. Wei, *eScience* **2022**, *2*, 445–452.

[53] H. Su, P. Gao, M. Y. Wang, G. Y. Zhai, J. J. Zhang, T. J. Zhao, J. Su, M. Antonietti, X. H. Li, J. S. Chen, *Angew. Chem. Int. Ed.* **2018**, *57*, 15194–15198.

[54] L. lai Liu, M. xuan Ma, H. Xu, X. ying Yang, X. yu Lu, P. Yang, H. Wang, *J. Electroanal. Chem.* **2022**, *920*, 116637.

[55] B. Goel, V. Vyas, N. Tripathi, A. Kumar Singh, P. W. Menezes, A. Indra, S. K. Jain, *ChemCatChem* **2020**, *12*, 5743–5749.